

## PAPER

# On ripples: bifurcations of resonant bimodal traveling waves

To cite this article: Benjamin F Akers 2025 *Nonlinearity* **38** 065005

View the [article online](#) for updates and enhancements.

## You may also like

- [Neutron detectors for the ESS diffractometers](#)  
I. Stefanescu, M. Christensen, J. Fenske et al.
- [Multitube monitors: a new-generation of neutron beam monitors](#)  
F. Lafont, D. Barkats, J.-C. Buffet et al.
- [Detector rates for the Small Angle Neutron Scattering instruments at the European Spallation Source](#)  
K. Kanaki, M. Klausz, T. Kittelmann et al.

# On ripples: bifurcations of resonant bimodal traveling waves

**Benjamin F Akers**

Department of Mathematics and Statistics, Air Force Institute of Technology, 2950  
Hobson Way, WPAFB, OH 45433, United States of America

E-mail: [benjamin.akers@us.af.mil](mailto:benjamin.akers@us.af.mil)

Received 22 November 2024; revised 3 April 2025

Accepted for publication 13 May 2025

Published 21 May 2025

Recommended by Dr Karima Khusnutdinova



CrossMark

## Abstract

The bifurcation structure of small amplitude bimodal periodic traveling capillary–gravity waves is discussed in a family of model equations. Wilton famously described this bifurcation when the two modes are in  $(1:m)$  harmonic resonance. He observed that branches of nonlinear solutions bifurcate from linear waves only near particular superpositions of the two harmonics. Recently, sheets of traveling ripples have been proven to exist near the resonant configuration with all but two ratios of the two modes, even in presences of  $(1:m)$  harmonic resonance. This paper addresses how Wilton’s branches of ripples are embedded within the sheets of bimodal ripples both asymptotically and numerically.

Keywords: ripples, bifurcations, waves, asymptotics

Mathematics Subject Classification numbers: 35B35, 76B15, 35P20

## 1. Introduction

The bifurcation structure of approximately bimodal  $(1:m)$  resonant periodic traveling waves in a family of weakly nonlinear models is investigated. The motivating equations model gravity–capillary water waves, for which these bimodal waves are historically referred to as Wilton ripples [1, 2]. Wilton noticed<sup>1</sup> that a singularity in Stokes’ expansion for traveling periodic water waves could be resolved with a Lyapunov–Schmidt procedure, using corrections to the ratio of two harmonics along with corrections to the wave speed to satisfy solvability conditions. Wilton’s framework has since been used to generate high order approximations [4],

<sup>1</sup> Harrison studied Wilton ripples slightly before Wilton did [3].

create numerical methods [5], and prove the existence of waves [6] and the analyticity of solution branches [7]. Wilton ripples have been computed in the water wave equations [8] and in approximate models [5, 9]. Most analytical studies focus on the case where the two modes take part in a second harmonic, that is a (1:2) resonance [10, 11]. The asymptotics of these waves grows more complicated with increased frequency difference. High frequency Wilton ripples were studied using Wilton's expansion in [12] and recently proven to exist in the Kawahara equation [13]. Experimental studies have been conducted for both the second harmonic and some higher frequency resonances [14–16]. The stability of these ripples has been studied numerically [17], and similar expansions have been used to study the spectrum of Stokes' waves [18–21].

In the last fifteen years, a number of authors have proven the existence of bimodal traveling waves using a combination of Lyapunov–Schmidt procedure and the implicit function theorem [22, 23]. Bimodal traveling waves have been shown to bifurcate from the resonant linear configuration in the gravity–capillary Whitham equation, using the Bond number as a bifurcation parameter rather than the ratio of the two primary modes [24]. The proof in [24] yields a proof of existence of sheets of traveling waves (rather than discrete branches), for all but two ratios of the two modes. This technique has also been applied to internal waves [25] and hydroelastic waves [26, 27].

In the gravity–capillary wave problem, the Bond number  $\sigma = \frac{\tau}{\rho g L^2}$  measures the relative importance of surface tension,  $\tau$ , to gravity,  $g$ , with  $\rho$  the density<sup>2</sup> and  $L$  a characteristic lengthscale [28]. The proof technique in [24–26] gives existence of branches of waves with all but two ratios of the two leading harmonics by allowing the Bond number to vary. Since classic Wilton ripples have fixed Bond number, it is not obvious that these sheets of waves include the classic Wilton ripple branches. For example, it would be possible based on the arguments in [24–26] that no bimodal waves with fixed Bond number exist.

The (1:2) resonant classic Wilton ripples have been shown to both exist [6] and be parametrically analytic [7] in the models equations discussed here. The proof technique in [7] is significantly more complicated for the (1: $m$ ) resonant Wilton ripples for  $m > 2$ . The variable Bond number proofs in [24–26] handle  $m > 2$  smoothly. The latter proof technique would thus be preferable to investigate the existence of high frequency resonant Wilton ripples in the venues where their existence is unknown, if only one could be sure that fixed Bond number branches were embedded within the sheets of waves.

In this work we study how the fixed Bond number branches of waves are embedded in the sheets of ripples. The asymptotics of branches bimodal resonant waves with fixed Bond number and sheets of waves with varying Bond number are developed and compared to numerical computations of the same. The classic branches of Wilton ripples, with fixed Bond number, are observed to be embedded within the sheets. As a venue for this study, the following family of weakly nonlinear models is used,

$$cu_x - \mathcal{L}u_x + (u^2)_x = 0. \quad (1)$$

The operator  $\mathcal{L}$  is defined via its multiplicative Fourier symbol,  $\widehat{\mathcal{L}(u)} = c_p(k)\hat{u}$ . The speed,  $c_p(k)$  is assumed to be a real, non-monotonic even function. Examples of model equations include the Kawahara equation  $c_p(k) = k^2 - \sigma k^4$  [29, 30], the Akers–Milewski equation  $c_p(k) = |k|^{-1} + \sigma|k|$  [31, 32], and the deep-water capillary–gravity Whitham equation  $c_p(k) =$

<sup>2</sup> Or density difference in internal wave problems.

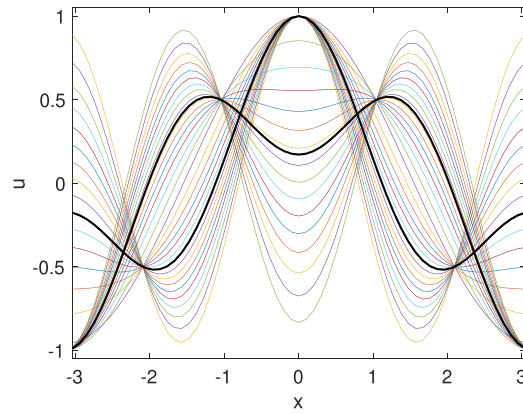


**Figure 1.** The small amplitude wave profiles on a sheet of triad ripples,  $n = 2$ , for  $\beta_1 = \tan(\theta)$  for  $\theta \in (\pi/2, \pi/2)$ , normalized by their maximum. The classic Wilton ripples are marked with thick solid black lines.

$(|k|^{-1} + \sigma|k|)^{1/2}$  [33, 34]. Asymptotic expansions of bimodal waves in the  $(1:m)$  harmonic resonant configuration will be developed. The form of the expansion when the Bond number is constant is contrasted to when the Bond number varies.

The paper is organized as follows. In section 2, the leading order asymptotics of  $(1:m)$  resonant traveling periodic ripples are developed. The asymptotics are developed with fixed Bond number as well as with varying Bond number. In section 3, a numerical quasi-Newton continuation procedure is described. Continuation procedures which mimic the asymptotics are used to calculate both sheets and fixed Bond number branches of waves. Conclusions and implications are presented in section 4.

## 2. Asymptotic expansions

Resonant bimodal waves, with two co-propagating modes, at frequencies  $k = 1$  and  $k = m$ , have asymptotics which begin

$$u = \epsilon (\cos(x) + \beta_1 \cos(mx)) + O(\epsilon^2) = \sum_{n=1}^{\infty} u_n \epsilon^n, \quad c = \sum_{n=0}^{\infty} c_n \epsilon^n.$$

That the lower frequency wave has frequency  $k = 1$  is a definition of the period cell, and would be part of the definition of the Bond number in the physical problem. The size parameter  $\epsilon$  is defined so that the solution has Fourier transform with  $\hat{u}(k = 1) = \epsilon/2$ . Thus the only term in the series which has nonzero projection onto  $\cos(x)$  is  $u_1$ . All later orders are orthogonal to  $\cos(x)$ . The parameter  $\beta_1$  is the ratio of the amplitudes of the two modes in  $u_1$ . Examples of such waves are plotted in figure 1.

This work studies the  $(1:m)$  harmonic resonant case, where the second frequency is an integer multiple of the first. These are the waves for which a classic Stokes expansion is singular. The circumstance where the two wavenumbers do not divide one another has also been studied [24–26]. When  $k = n$  and  $k = m$  with  $\frac{n}{m} \notin \mathbb{Z}$ , a classic Stokes’ wave expansion allows for waves which are supported solely at either frequency. Allowing the Bond number to vary near such a configuration allows for arbitrary superposition of the two modes [24–26]. Such waves are not in harmonic resonance and will not be considered here.

The linear  $O(\epsilon)$  problem allows for arbitrary  $\beta_1$  and  $c_0 = c_p(1)$ . In order for the two modes to co-propagate, one requires  $c_p(1) = c_p(m)$ . The remainder of the expansion depends on which parameters vary with wave amplitude. We consider two expansions, when the Bond number is held constant, as in [1, 2, 6, 7], and when it is permitted to vary, as in [24–26]. Both expansions will be calculated in the integrated form of (1),

$$(c - \mathcal{L})u + P\{u^2\} = 0. \tag{2}$$

The constant of integration is set to zero. Nonzero values for this constant can be absorbed by redefining the speed and mean. The operator  $P$  is the projection which removes the mean.

### 2.1. Wilton ripples

The classic choice is to keep the Bond number fixed, and allow the ratio of the elements of the kernel of the operator,  $(c_0 - \mathcal{L})$ , to vary along the branch [1–3]. Another common choice is to focus on the case where the two co-propagating modes have wavenumbers  $k = 1$  and  $k = 2$ , the triad ripple, a (1:2) resonance [10, 35], which we consider first. The asymptotics can be calculated in the following series expansion for  $u(x)$ ,

$$u = \epsilon (\cos(x) + \beta_1 \cos(2x)) + \epsilon^2 (u_{2,p} + \beta_2 \cos(2x)) + \epsilon^3 (u_{3,p} + \beta_3 \cos(2x)) + \dots, \tag{3}$$

in which  $u_{n,p}$  are orthogonal to both  $\cos(x)$  and  $\cos(2x)$ . This series implicitly defines  $\epsilon$  as the projection of the solution onto  $\cos(x)$ , and  $\beta = \sum_{n=1}^{\infty} \epsilon^n \beta_n$  the projection onto  $\cos(2x)$ . The projection onto  $\cos(x)$  is chosen instead of the projection onto  $\cos(2x)$  as the former is presumed nonzero when in the definition of the period cell. This definition is convenient for the asymptotics; one does not need to include  $\cos(x)$  terms at each correction order. If one instead makes the more general choice,

$$u = \sum_{n=1}^{\infty} \tilde{\epsilon}^n \left( \tilde{u}_{n,p} + \alpha_n \cos(x) + \tilde{\beta}_n \cos(2x) \right),$$

the transformation

$$\epsilon = \sum_{n=1}^{\infty} \tilde{\epsilon}^n \alpha_n,$$

results in a solution of the form of (3).

The full series can be formally computed via Lyapunov–Schmidt reduction, the  $\beta_n$  and  $c_n$  are used to satisfy solvability conditions. First, the  $O(\epsilon^2)$  problem is

$$(c_0 - \mathcal{L})u_{2,p} = -c_1 u_1 - P\{u_1^2\}. \tag{4}$$

The operator  $(c_0 - \mathcal{L})$  is self-adjoint, with null space  $\{\cos(x), \cos(2x)\}$ . Defining the inner product,

$$\langle f, g \rangle = \frac{1}{\pi} \int_0^{2\pi} f g dx,$$

the solvability conditions for (4) are

$$c_1 + \beta_1 = 0 \quad \text{and} \quad c_1 \beta_1 + 1/2 = 0.$$

Equation (4) is thus solvable only when for  $\beta_1 = \pm\sqrt{1/2}$ ,  $c_1 = \mp\sqrt{1/2}$ . Later orders have linear solvability conditions, see [4, 5]. The series is summable and thus these branches are parametrically analytic [7]. The important feature for later comparison is that only two values of  $\beta_1$  are permitted when the Bond number is fixed.

2.2. High frequency ripples

When a Wilton ripple has higher frequency resonant mode,  $m > 2$ , the amplitude of this mode is determined at  $O(\epsilon^3)$ . In this case, the solution has form

$$u = \epsilon (\cos(x) + \beta_1 \cos(mx)) + \epsilon^2 (u_{2,p} + \beta_2 \cos(mx)) + \epsilon^3 (u_{3,p} + \beta_3 \cos(mx)) + \dots$$

The  $O(\epsilon^2)$  equation is

$$(c_0 - \mathcal{L})u_2 + c_1 u_1 + P\{u_1^2\} = 0,$$

which is solvable when  $c_1 = 0$  for arbitrary  $\beta_1$ . The correction  $u_2$  is

$$u_2 = \beta_2 \cos(mx) - \frac{\cos(2x)}{2(c_0 - c_p(2))} - \frac{\beta_1 \cos((m+1)x)}{c_0 - c_p(m+1)} - \frac{\beta_1 \cos((m-1)x)}{c_0 - c_p(m-1)} - \frac{\beta_1^2 \cos(2mx)}{2(c_0 - c_p(2m))}.$$

The  $O(\epsilon^3)$  equation is

$$(c_0 - \mathcal{L})u_3 + c_2 u_1 + 2P\{u_1 u_2\} = 0.$$

The solvability conditions are

$$c_2 = \frac{1 + \beta_1 \delta_{m,3}}{2(c_0 - c_p(2))} + \frac{\beta_1 \delta_{m,3} + \beta_1^2}{c_0 - c_p(m-1)} + \frac{\beta_1^2}{c_0 - c_p(m+1)}$$

and

$$c_2 \beta_1 = \frac{\delta_{m,3}}{2(c_0 - c_p(2))} + \frac{\beta_1}{c_0 - c_p(m+1)} + \frac{\beta_1}{c_0 - c_p(m-1)} + \frac{\beta_1^3}{2(c_0 - c_p(2m))},$$

in which  $\delta_{m,3}$  is a Kronecker delta function. These solvability conditions imply a cubic equation for  $\beta_1$ ,

$$\begin{aligned} & \left( \frac{1}{c_0 - c_p(m+1)} + \frac{1}{c_0 - c_p(m-1)} - \frac{1}{2(c_0 - c_p(2m))} \right) \beta_1^3 \\ & + \delta_{m,3} \left( \frac{1}{2(c_0 - c_p(2))} + \frac{1}{c_0 - c_p(m-1)} \right) \beta_1^2 \\ & + \left( \frac{1}{2(c_0 - c_p(2))} - \frac{1}{c_0 - c_p(m-1)} - \frac{1}{c_0 - c_p(m+1)} \right) \beta_1 \\ & + \delta_{m,3} \left( \frac{1}{2(c_0 - c_p(2))} \right) = 0. \end{aligned} \tag{5}$$

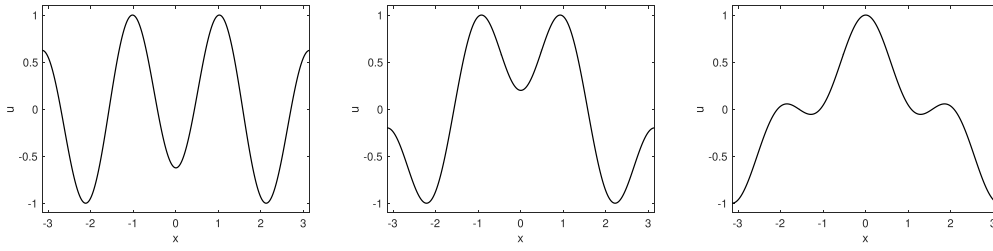


**Figure 2.** Examples of waves from three branches of high-frequency Wilton ripples with  $m = 3$  in the deep water gravity–capillary Whitham equation, normalized by their maxima.

For  $m > 3$  this cubic is simple to factor, with roots  $\beta_1 = 0$  and

$$\beta_1 = \pm \sqrt{\frac{\left(\frac{1}{2(c_0 - c_p(2))} - \frac{1}{c_0 - c_p(m+1)} - \frac{1}{c_0 - c_p(m-1)}\right)}{\left(\frac{1}{2(c_0 - c_p(2m))} - \frac{1}{c_0 - c_p(m+1)} - \frac{1}{c_0 - c_p(m-1)}\right)}}. \tag{6}$$

For the named models (the Kawahara equation, the deep water gravity–capillary Whitham equation, and the Akers–Milewski equation), the two non-zero values of  $\beta_1$  are both observed to be imaginary for  $m \in [4, 10]$ . It is possible for  $\beta_1$  to be real and nonzero for  $m > 3$ ; The toy model  $\hat{\mathcal{L}} = -|k| + \sigma|k|^3$  with  $\sigma = (n^2 + n + 1)^{-1}$ , supports two real values when  $m = 4$  with  $\beta_1 \approx \pm 0.2143$ . When the asymptotics allow only a single real value of  $\beta_1$ , they predict a single branch of waves bifurcating from the flat state. This branch may contain support at wavenumber  $k = m$ , but not at leading order in  $\epsilon$  (for example  $\beta_3$  may be nonzero but not  $\beta_1$ ). Examples of wave profiles with  $m=3$  are in figure 2.

Throughout this work we ignore the branches of Stokes waves at wavenumber  $k = m$  which have no support at wavenumber  $k = 1$ . We argue that these waves have a smaller fundamental period, which would be reflected in the definition of the Bond number. The classic Stokes’ expansion has no singularity in this case. If one is interested in describing all bifurcations from all linear solutions at the Bond numbers of this paper this branch of waves should also be considered. If the Stokes wave at  $k = m$  is included then each bifurcation described above has exactly one more branch of solutions.

### 2.3. Sheets

In this section, the asymptotics of sheets of bimodal traveling waves are developed. These sheets of traveling waves are the union of branches of traveling waves at varying amplitude, each of which has speed and Bond number which are expanded in amplitude. The ratio of the leading modes,  $\beta_1$ , is left free and dictates which branch is followed. This procedure builds branches of traveling waves which are, by their form, assumed to be analytic in amplitude. As parametric analyticity is a stronger restriction than the smoothness guaranteed by the theorems in [24–26], it is possible that these asymptotics describe only a subset of those solutions. In either case, we observe that the classic Wilton ripple branches, with constant Bond number, lie within the sheets described below.

We begin by describing the triad ripple, (1:2) resonant configuration. The solution is expanded as a parametrically analytic series in amplitude,

$$u = \epsilon (\cos(x) + \beta_1 \cos(2x)) + O(\epsilon^2) = \sum_{n=1}^{\infty} u_n \epsilon^n, \quad c = \sum_{n=0}^{\infty} c_n \epsilon^n.$$

The sheets of waves are also calculated with Lyapunov–Schmidt reduction, just like the branches of classic Wilton ripples. At each order, the  $c_n$  are used for one of the solvability conditions. For the second condition solvability condition, the Bond number is expanded,

$$\sigma = \sum \sigma_n \epsilon^n.$$

As the Bond number only enters the problem in  $\mathcal{L}$ , this requires the operator be expanded,

$$\mathcal{L}(\sigma) = \mathcal{L}(\sigma_0) + \frac{\partial \mathcal{L}}{\partial \sigma}(\sigma_0) \epsilon \sigma_1 + O(\epsilon^2). \tag{7}$$

To calculate the operators in the expansion, e.g.  $\frac{\partial \mathcal{L}}{\partial \sigma}$ , the partial derivatives are taken of the Fourier symbols. For example, in deep water Whitham,  $\hat{\mathcal{L}}(k, \sigma) = \sqrt{\frac{1}{|k|} + \sigma|k|}$ , so that  $\frac{\partial \hat{\mathcal{L}}}{\partial \sigma}(k, \sigma_0) = \frac{1}{2}(|k|^{-1} + \sigma_0|k|)^{1/2}|k|$ . In the Kawahara and Akers–Milewski equations the operator expansion (7) is exact after one term; for Whitham, this expansion is infinite. It is natural to question whether the operator’s expansion converges; this work is restricted to the formal asymptotics. The  $O(\epsilon^2)$  problem is

$$(c_0 - \mathcal{L})u_2 + \left( c_1 - \sigma_1 \frac{\partial \mathcal{L}}{\partial \sigma}(\sigma_0) \right) u_1 + P \{u_1^2\} = 0, \tag{8}$$

whose solvability conditions require that

$$\begin{pmatrix} 1 & -\frac{\partial \hat{\mathcal{L}}(1, \sigma_0)}{\partial \sigma} \\ \beta_1 & -\beta_1 \frac{\partial \hat{\mathcal{L}}(2, \sigma_0)}{\partial \sigma} \end{pmatrix} \begin{pmatrix} c_1 \\ \sigma_1 \end{pmatrix} = - \begin{pmatrix} \beta_1 \\ 1/2 \end{pmatrix}. \tag{9}$$

The solution to the (9) gives the below corrections to the speed and Bond number,

$$\sigma_1 = \frac{\beta_1^2 - 1/2}{\beta_1 \left( \frac{\partial \hat{\mathcal{L}}(1, \sigma_0)}{\partial \sigma} - \frac{\partial \hat{\mathcal{L}}(2, \sigma_0)}{\partial \sigma} \right)}, \quad c_1 = \frac{\beta_1^2 \frac{\partial \hat{\mathcal{L}}(2, \sigma_0)}{\partial \sigma} - \frac{1}{2} \frac{\partial \hat{\mathcal{L}}(1, \sigma_0)}{\partial \sigma}}{\beta_1 \left( \frac{\partial \hat{\mathcal{L}}(1, \sigma_0)}{\partial \sigma} - \frac{\partial \hat{\mathcal{L}}(2, \sigma_0)}{\partial \sigma} \right)}.$$

These corrections (and the rest of the series) formally exist, provided

$$\beta_1 \neq 0 \quad \text{and} \quad \left( \frac{\partial \hat{\mathcal{L}}(1, \sigma_0)}{\partial \sigma} - \frac{\partial \hat{\mathcal{L}}(2, \sigma_0)}{\partial \sigma} \right) \neq 0.$$

The condition on the linear operators is satisfied for the three named equations considered here (Kawahara, Deep Water Whitham and Akers–Milewski). The matrix in (9) is populated with the first variations of the problem with respect to  $c$  and  $\sigma$  evaluated at the two wavenumbers. The invertibility of such a matrix is precisely what one would expect to need for the local existence of solutions to this problem. An analogous matrix must be invertible in the implicit function based proofs of existence of ripples, for example the matrix in equation (57) in [26]. This invertibility is not something that can be guaranteed for all models, but must be checked for each case. That this matrix is not invertible for  $\beta_1 = 0$  is responsible for the wedge punctured from the disc of solutions guaranteed in [24–26].

The value of  $\sigma_1$  is nonzero except for  $\beta_1 = \pm\sqrt{1/2}$ , the leading second harmonic coefficient of Wilton ripples. When  $\beta_1 = \pm\sqrt{1/2}$ , the speed correction reduces to  $c_1 = \mp\sqrt{1/2}$  again recovering the Wilton ripple value. These asymptotics suggest two things. First, that the classic, constant surface tension Wilton ripple is within the sheets whose existence is proven in [24–26]. Second, the only values of  $\beta_1$  for which the a branch of waves embedded within these sheets can have constant Bond number are the values required in the classic expansion.

In both circumstances the asymptotics do not prove the existence of these waves, however existence proofs already exist in the (1:2) resonant case both for the sheets [24–26] and for the fixed Bond number [6, 7].

### 2.4. High frequency sheets

For  $m > 2$  the asymptotics of the sheets differ from the  $m = 2$  case, but all share a common structure.

$$u = \epsilon (\cos(x) + \beta_1 \cos(mx)) + \epsilon^2 (u_{2,p} + \beta_2 \cos(mx)) + \epsilon^3 u_3 + \dots$$

The  $O(\epsilon^2)$  equation for  $u_{2,p}$  is still (8), but the solvability conditions now give  $\sigma_1 = c_1 = 0$ . The solution to (8) is now

$$u_2 = \beta_2 \cos(mx) - \frac{1}{2(c_0 - c_p(2))} \cos(2x) - \frac{\beta_1^2}{2(c_0 - c_p(2m))} \cos(2mx) - \dots \quad (10)$$

$$\frac{\beta_1}{c_0 - c_p(m+1)} \cos((m+1)x) - \frac{\beta_1}{c_0 - c_p(m-1)} \cos((m-1)x).$$

The  $O(\epsilon^3)$  equation is

$$(c_0 - \mathcal{L})u_3 = - \left( c_2 - \sigma_2 \frac{\partial \mathcal{L}}{\partial \sigma}(\sigma_0) \right) u_1 - 2P\{u_2 u_1\}, \quad (11)$$

which has solvability conditions,

$$\begin{pmatrix} 1 & -\frac{\partial \hat{\mathcal{L}}(1, \sigma_0)}{\partial \sigma} \\ \beta_1 & -\beta_1 \frac{\partial \hat{\mathcal{L}}(m, \sigma_0)}{\partial \sigma} \end{pmatrix} \begin{pmatrix} c_2 \\ \sigma_2 \end{pmatrix} = \begin{pmatrix} \frac{1}{2(c_0 - c_p(2))} + \frac{\beta_1 \delta_{m,3}}{2(c_0 - c_p(2))} + \frac{\beta_1 \delta_{m,3}}{c_0 - c_p(m-1)} + \frac{\beta_1^2}{c_0 - c_p(m-1)} + \frac{\beta_1^2}{c_0 - c_p(m+1)} \\ \frac{\delta_{m,3}}{2(c_0 - c_p(2))} + \frac{\beta_1}{c_0 - c_p(m+1)} + \frac{\beta_1}{c_0 - c_p(m-1)} + \frac{\beta_1^3}{2(c_0 - c_p(2m))} \end{pmatrix}.$$

The solutions to this system are

$$\sigma_2 = \frac{1}{\beta_1 \left( \frac{\partial \hat{\mathcal{L}}(m, \sigma_0)}{\partial \sigma} - \frac{\partial \hat{\mathcal{L}}(1, \sigma_0)}{\partial \sigma} \right)} \left( \frac{\beta_1 + (\beta_1^2 - 1) \delta_{m,3}}{2(c_0 - c_p(2))} + \frac{\beta_1^3 - \beta_1 + \beta_1^2 \delta_{m,3}}{c_0 - c_p(m-1)} + \frac{\beta_1^3 - \beta_1}{c_0 - c_p(m+1)} - \frac{\beta_1^3}{2(c_0 - c_p(2m))} \right) \quad (12)$$

Notice that  $\sigma_2 = 0$  when

$$\begin{aligned} & \left( \frac{1}{c_0 - c_p(m-1)} + \frac{1}{c_0 - c_p(m+1)} - \frac{1}{2(c_0 - c_p(2m))} \right) \beta_1^3 \\ & + \delta_{m,3} \left( \frac{1}{2(c_0 - c_p(2))} + \frac{1}{c_0 - c_p(m-1)} \right) \beta_1^2 \\ & + \left( \frac{1}{2(c_0 - c_p(2))} - \frac{1}{c_0 - c_p(m+1)} - \frac{1}{c_0 - c_p(m-1)} \right) \beta_1 \\ & + \delta_{m,3} \left( \frac{1}{2(c_0 - c_p(2))} \right) = 0 \end{aligned} \quad (13)$$

which is the same condition on  $\beta_1$  required for the existence of the high frequency Wilton ripple branches in (5). When  $n > 3$  equation (12) is undefined at  $\beta_1 = 0$ ; this is the manifestation of the wedge for which the proofs in [24–26] do not guarantee the existence of waves. On the other hand, the solvability conditions for  $n > 3$  allow for  $\sigma_2 = 0$  and  $\beta_1 = 0$ . In the numerical section we observe the existence of fixed Bond number waves with  $\beta_1 = 0$  in these cases.

The asymptotics of the sheets of waves can be understood in the context of resonant interaction theory [36, 37]. Resonant interaction theory considers the time dynamics of a superposition of small amplitude of near-sinusoidal waves via a system of equations for the wave amplitudes [2, 38]. The amplitude equations are closed at a finite collection of modes when the spatial and temporal frequencies of the waves satisfies a pair of resonance conditions. These conditions are hierarchically labeled, by the order at which they appear in an asymptotic expansion. Triad, or three-wave, resonances come before the four-wave resonant quartets; quartets come before quintets and so forth. The amplitude equations can then be used to predict the stability and dynamics of small amplitude solutions [39, 40]. The leading asymptotics of the sheets of traveling waves follow a predictable pattern when viewed in the context of resonant interaction theory, as these same resonances are responsible for the first non-zero corrections.

For the  $m = 2$  case,  $c_1$  and  $\sigma_1$  are the first nonzero corrections because the waves  $k_1 = 1$  and  $k_2 = 2$  participate in a degenerate triad resonance,

$$k_1 + k_1 = k_2, \quad \text{and} \quad \omega_1 + \omega_1 = \omega_2.$$

For  $m > 2$ , the corrections  $c_2$  and  $\sigma_2$  are the first nonzero corrections because the wave numbers take part in a resonant quartet (but not a triad). Resonant quartets exist between every pair of wavenumbers,  $k_1 = 1$  and  $k_2 = m$ . These include a quartet interaction of  $k_1$  and  $k_2$ ,

$$k_1 + k_2 - k_2 = k_1, \quad \text{and} \quad \omega_1 + \omega_2 - \omega_2 = \omega_1,$$

as well as an interaction of  $k_1$  with itself,

$$k_1 + k_1 - k_1 = k_1, \quad \text{and} \quad \omega_1 + \omega_1 - \omega_1 = \omega_1,$$

and the interaction of  $k_2$  with itself,

$$k_2 + k_2 - k_2 = k_2, \quad \text{and} \quad \omega_2 + \omega_2 - \omega_2 = \omega_2.$$

The above quartets exist for every  $m$ . When  $m = 3$  an additional quartet interaction exists,

$$k_2 = k_1 + k_1 + k_1 \quad \text{and} \quad \omega_1 + \omega_1 + \omega_1 = \omega_2.$$

This last interaction is responsible for the terms with  $\delta_{m,3}$  in (13). When  $m = 2$  the triad interaction results in nonzero  $\sigma_1$ ; when  $m > 2$  there are no triads but quartet interactions cause  $\sigma_2$  to be nonzero. For all higher frequencies,  $m \geq 3$  the leading order asymptotics are still dictated by quartet interactions causing nonzero  $\sigma_2$ . The first nonzero  $\sigma_j$  does not occur at later orders as  $m$  increases, the first nonzero  $\sigma_j$  is  $\sigma_2$  for  $m > 2$  for all but the special  $\beta_1$  for which Wilton ripples exist. One could in principle calculate the Wilton ripple  $\beta_1$  values by computing sheets of waves and then finding the values of  $\beta_1$  for which  $\frac{\partial \sigma}{\partial \epsilon} = 0$ .

### 3. Numerical simulations

To complement, and verify, the asymptotics of the previous section, branches of Wilton ripples and sheets of ripples are computed numerically. The numerical method is a quasi-Newton iteration for the Fourier modes of the traveling wave, complemented by continuation in amplitude. The numerical solution is represented

$$u_M = \sum_{p=-M/2}^{M/2} a_p \exp(ipx)$$

Real, even solutions are sought with  $a_p = a_{-p}$ . The mean of  $u(x)$  is set to zero (nonzero mean can be absorbed into the definition of  $c$ ). The speed is also computed as part of the solution. When computing branches of Wilton ripples with fixed  $\sigma$ , the Newton solver is seeking  $M/2$  Fourier modes and the speed  $c$ . When computing sheets, the  $m$ th harmonic's coefficient  $a_m$  is specified (one less unknown), but the Bond number  $\sigma$  is then part of the solution, so the total number of unknowns is the same in both cases. The total displacement  $h = \max(u) - \min(u)$  is used as a continuation parameter. This numerical procedure uses the asymptotics of the previous section only for initial guesses, so as to provide independent validation of the asymptotic predictions.

Two distinct continuation procedures are conducted. First, branches of Wilton ripples are computed, using the initial guess  $u = A(\cos(x) + \beta_1 \cos(mx))$  with  $\beta_1$  initialized using the special values from section 2.1. The amplitude of the first guess,  $A$ , is set at  $10^{-5}$ . These branches have fixed  $\sigma$ , and classic Wilton ripples are computed continuing in speed and amplitude as in [41]. This procedure results in two or three branches of waves depending on the type of resonance involved, similar to the computations in [5, 12].

The second continuation procedure is used to compute sheets of waves. The same guess for the wave is used,  $u = A(\cos(x) + \beta \cos(mx))$ , but now  $\beta = \tan(\theta)$  is varied over a sampling of  $\theta \in (\pi/2, \pi/2)$ . The amplitude of the first guess,  $A$ , is set at  $10^{-5}$ . In these computations the ratio of the wave's  $m$ th to its first Fourier coefficient is specified, rather than solved for so the ratio  $\beta$  is fixed.

When the Bond number is allowed to vary, as in the sheets of waves in 2.3, one need not expand  $\beta$  as a function of  $\epsilon$ ; the solvability conditions are satisfied using speed and Bond number corrections. These waves exist when  $\beta = \beta_1$ . In the notation of the previous sections, the numerical computations of sheets take  $\beta = \sum_{j=1}^{\infty} \beta_j e^{j-1} = \beta_1$ . The Bond number,  $\sigma$ , is initialized by the value for which the linear problem has two-dimensional kernel. The ratio of the two harmonics  $\beta$ , is fixed and dictates the direction within the sheet along which a branch of waves is computed. Each branch is computed by continuation in speed, amplitude and Bond number with fixed  $\beta$ . A sheet is constructed as a union of branches for each sampled  $\beta$ . Examples of sheets constructed with this method are in figures 5–7. The waves computed here are very small amplitude with rapidly decaying Fourier series;  $N_x = 32$  is observed to be more than sufficient to resolve the waves to machine precision.

The numerical computations of sheets of waves were used to estimate the first corrections to the Bond number within the sheet. For  $m = 2$ , the asymptotic prediction is that  $\sigma_1$  is nonzero. The first derivative of  $\sigma$  with respect to  $\epsilon$  was numerically computed via finite difference between the first two waves on a branch (with  $\epsilon \approx 10^{-5}$ ). The numerical estimates are compared to the asymptotic prediction for three example model equations in figure 3. In all three models the two computations of  $\sigma_1$  match to the precision of graph. Also marked in this figure are the values of  $\beta_1$  for which  $\sigma_1$  vanishes, the classic Wilton ripple ratios.

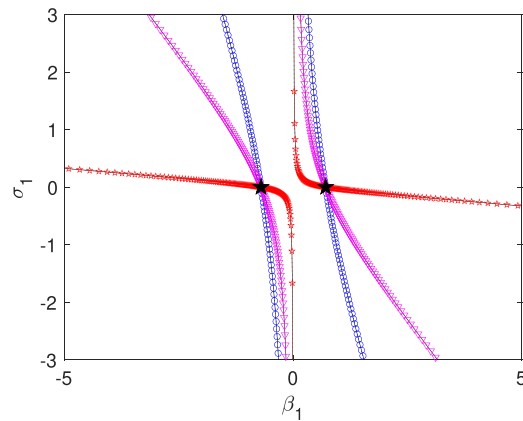


**Figure 3.** The asymptotic calculation of  $\sigma_1(\beta_1)$  for triad ripples,  $m = 2$ , (solid line) compared to numerical calculations of the same by a finite difference calculation along a branch (markers). These curves agree to the precision of this graphic. The numerical approximations are marked with blue circles for the gravity–capillary deep water Whitham equation, pink triangles for the Akers–Milewski equation, and red stars for the Kawahara equation. The Wilton ripples value  $\beta_1 = \pm\sqrt{1/2}$  are the roots of  $\sigma_1$  for all three models (marked with black solid stars).

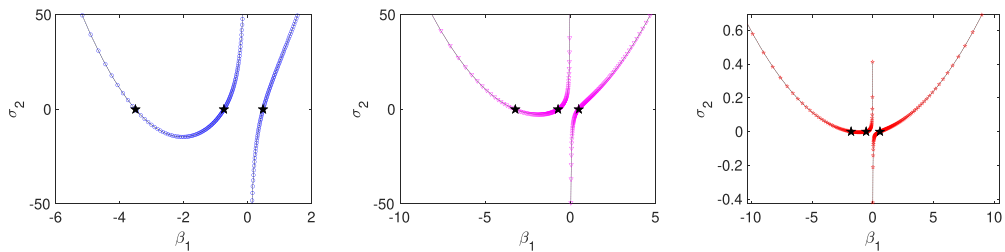


**Figure 4.** The asymptotic calculation of  $\sigma_2(\beta_1)$  for quartet ripples,  $n = 3$ , (solid line) compared to numerical calculations of the same by a finite difference calculation along a branch (markers). These curves agree to the precision of these graphics. The numerical approximations are marked with blue circles for the deep water Whitham equation, pink triangles for the Akers–Milewski equation, and red stars for the Kawahara equation. The Wilton ripples values of  $\beta_1$  are the roots of  $\sigma_2$  for all three models (marked with black solid stars).

When  $m = 3$  the leading correction to the Bond number is  $\sigma_2$ . The numerical computations of sheets of waves were also used to computed estimates to  $\sigma_2$ , with a centered difference estimate of the second derivative of  $\sigma$  with respect to  $\epsilon$ . This calculation used the first three waves on branch (with  $\epsilon \approx 10^{-5}$ ). This numerical estimate of  $\sigma_2$  is compared to the asymptotic predictions of the same in figure 4. The two estimates match to the precision of the graph for three example model equations. Also marked in this figure are the three values of  $\beta_1$  for which  $\sigma_2$  vanishes.

In figures 5–7 the sheets of bifurcated waves are visualized in the three dimensional amplitude, Bond number and mode ratio  $(\epsilon, \sigma, \beta)$  space. Each figure depicts a different class of bifurcation. The colored sheets were computed using quasi-Newton iteration and continuation which fixed  $\beta$  with  $\sigma$  an unknown. When classic, fixed Bond number, Wilton ripples exist,

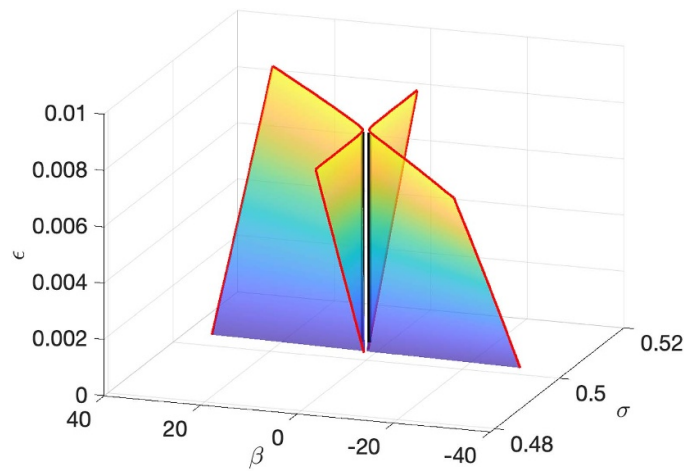


**Figure 5.** The two surfaces of triad, (1:2) resonant, traveling waves which bifurcate from  $\sigma = 1/2, \epsilon = 0$  in the deep water gravity–capillary Whitham equation are depicted. The surfaces use  $\beta = \tan(\theta)$  for  $\theta \in (-\pi/2 + 0.02, 0.02)$  and  $\theta \in (0.02, \pi/2 - 0.02)$ . There is a gap in the surfaces corresponding to  $\beta = 0$ , waves with no second harmonic. The classic triad Wilton ripple,  $\beta_1 = \pm\sqrt{1/2}$  has  $\sigma \equiv 1/2$ ; these branches are marked with a solid black line.

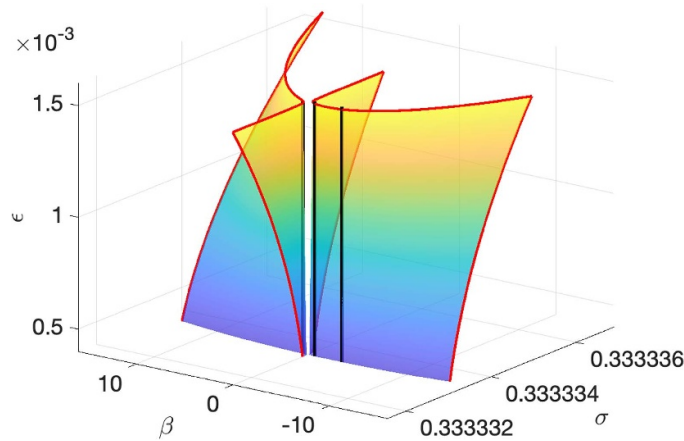


**Figure 6.** The two surfaces of quartet, (1:3) resonant, traveling waves which bifurcate from  $\sigma = 1/3, \epsilon = 0$  in the deep water gravity–capillary Whitham equation are depicted. The surfaces were initialized using  $\beta = \tan(\theta)$  for  $\theta \in (-\pi/2 + 0.02, 0.02)$  and  $\theta \in (0.02, \pi/2 - 0.02)$ . There is a gap in the surfaces corresponding to  $\theta = 0$ , waves with no third harmonic. The quartet,  $n = 3$ , Wilton ripple branches are marked with a solid black line and have  $\sigma \equiv 1/3$ .

these were computed using a quasi-Newton iteration and continuation with  $\sigma$  fixed and  $\beta$  unknown. These waves are marked with solid black lines.

Figure 5 depicts a triad (1:2) resonant bifurcation. At zero amplitude in this figure, the waves all have  $\sigma = 0.5$ . The mode ratio,  $\beta$ , varies through all values save  $\beta = 0$ . At small amplitude the sheet is a horizontal line with a gap at  $\beta = 0$ . For larger amplitude, the sheet departs  $\sigma = 0.5$

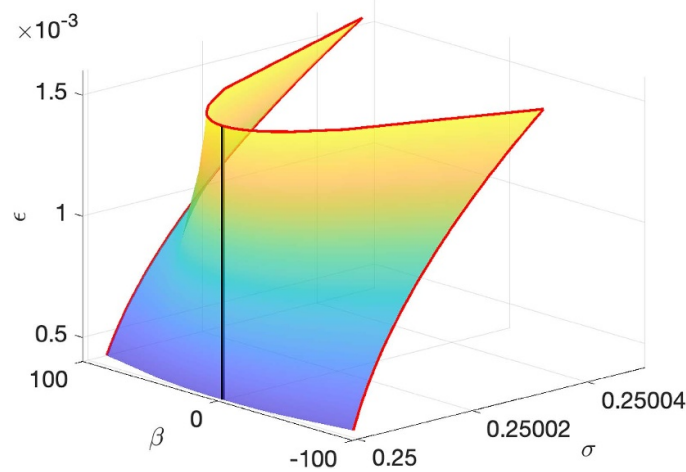


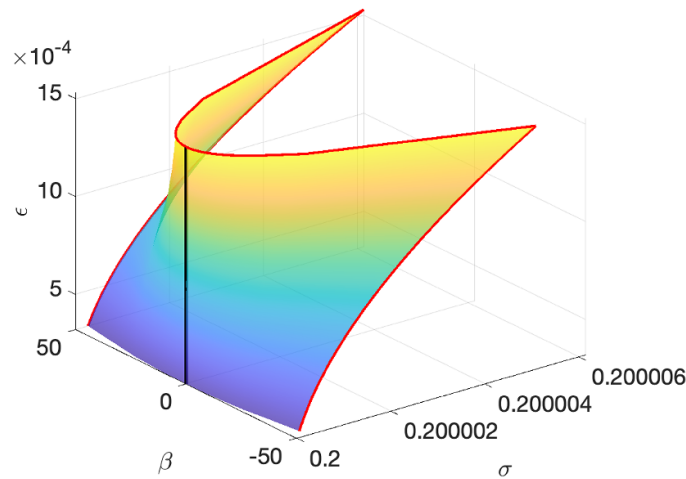
**Figure 7.** A sheet of quintet, (1:4) resonant, traveling waves which bifurcate from  $\sigma = 1/4, \epsilon = 0$  in the deep water gravity–capillary Whitham equation are depicted. The surface was initialized using  $\beta = \tan(\theta)$  for  $\theta \in (-\pi/2 + 0.02, \pi/2 - 0.02)$ . There is a single branch of waves with constant Bond number,  $\sigma$ , with  $\beta_1 = 0$ .

at all values of  $\beta$  except two  $\beta = \pm\sqrt{1/2}$ . Branches of classic Wilton ripples computed with fixed  $\sigma$  are marked with solid black lines.

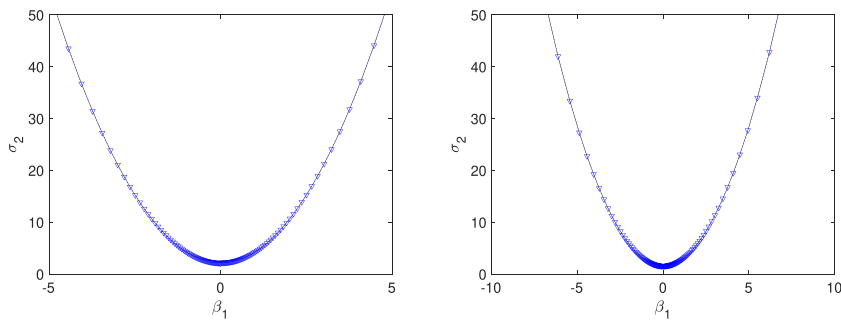
Figure 6 depicts a quartet (1:3) resonant bifurcation. At zero amplitude in this figure, the waves all have  $\sigma = 1/3$ . The mode ratio,  $\beta$ , varies through all values save  $\beta = 0$ . At small amplitude the sheet is a horizontal line with a gap at  $\beta = 0$ . For larger amplitude, the sheet departs  $\sigma = 1/3$  except three special values of  $\beta$ . Branches of classic Wilton ripples computed with fixed  $\sigma$  are marked with solid black lines, and correspond to these three special values.

Figure 7 depicts a quintet (1:4) resonant bifurcation. At zero amplitude in this figure, the waves all have  $\sigma = 0.25$ . The mode ratio,  $\beta$ , varies through all values including  $\beta = 0$ . At small amplitude the sheet is a horizontal line with no gap. Notice that in the asymptotic prediction of (12) the value  $\beta = 0$  yields an indeterminate value for  $\sigma_2$  for  $m > 3$ . The numerical computations here show that this value does not create a gap in the sheet, but rather then sheet is continuously connected through the value  $\beta = 0$ . For larger amplitude, the sheet departs  $\sigma = 0.25$  at all values of  $\beta$  except  $\beta = 0$ , for which a fixed Bond number expansion predicts a wave with no fourth harmonic. In this configuration, (6) predicts that no classic Wilton ripples exist with nonzero  $\beta_1$ . The numeric computations of the sheets confirms this prediction, no waves in the sheet have fixed Bond number except  $\beta = 0$ .

The case  $\beta = 0$  for  $m > 3$  is of special interest because the theorems in [24–26] do not guarantee the existence of waves for  $\beta = 0$ . The numerical computations of this paper calculate continuous sheets of waves, see figures 7 and 8, with no gap at  $\beta_1 = 0$ . Examples of the dependence of  $\sigma_2$  when  $m > 3$  is depicted in figure 9. Notice that this correction vanishes at  $\beta_1 = 0$ , and is a continuous function of  $\beta_1$ . This suggests that the gap in the proofs in [24–26] at  $\beta = 0$  then  $m > 3$  is not an absence of solutions, but instead a configuration that the proof technique cannot handle.



**Figure 8.** A sheet of sextet, (1:5) resonant, traveling waves which bifurcate from  $\sigma = 1/5, \epsilon = 0$  in the deep water gravity–capillary Whitham equation are depicted. The surface was initialized using  $\beta = \tan(\theta)$  for  $\theta \in (-\pi/2 + 0.02, \pi/2 - 0.02)$ . There is a single branch of waves with constant Bond number,  $\sigma$ , which occurs when  $\beta_1 = 0$ .



**Figure 9.** Left: the asymptotic calculation of  $\sigma_2(\beta_1)$  for quintet resonant waves,  $n = 4$ , (solid line) compared to numerical calculations of the same by a finite difference calculation along a branch (triangles). Right: the asymptotic calculation of  $\sigma_2(\beta_1)$  for sextet resonant waves,  $n = 5$ , (solid line) compared to numerical calculations of the same by a finite difference calculation along a branch (triangles). Both computations are in the deep water gravity–capillary Whitham equation. These curves agree to the precision of this graphic.

#### 4. Conclusion

Two different presentations of bifurcations of (1: $m$ ) harmonic resonant bimodal traveling waves are developed. Classic Wilton ripples, with fixed Bond number, are included in both presentations. The leading order asymptotics of the bifurcation is presented with fixed Bond number, in which case only particular ratios of the two modes are permitted. The leading asymptotics are also presented when the Bond number is expanded, in which case all ratios of the two modes are permitted save one. In the latter expansion, the mode ratio is essentially a free parameter, thus this bifurcation yields sheets of traveling waves, rather than discrete branches. The asymptotics of the sheets of waves have Bond numbers which do not vary with

amplitude at the crucial ratios suggesting that the classic Wilton ripples are embedded within the sheets. Numerical simulations designed to follow both asymptotic approaches support this conclusion. When the waves are in  $(1:m)$  resonance with  $m > 3$ , the sheets are observed to be continuous, which the proofs in [24–26] do not guarantee.

### Data availability statement

All data that support the findings of this study are included within the article (and any supplementary files).

### References

- [1] Wilton J R 1915 LXXII. On Ripples *London, Edinburgh Dublin Phil. Mag. J. Sci.* **29** 688–700
- [2] McGoldrick L F 1965 Resonant interactions among capillary-gravity waves *J. Fluid Mech.* **21** 305–31
- [3] Harrison W J 1909 The influence of viscosity and capillarity on waves of finite amplitude *Proc. Math. Soc.* **2** 107–21
- [4] Akers B F 2016 High-order perturbation of surfaces short course: traveling water waves *Lect. Theor. Water Waves* **426** 19–31
- [5] Akers B F and Gao W 2012 Wilton ripples in weakly nonlinear model equations *Commun. Math. Sci.* **10** 1015–24
- [6] Akers B and Nicholls D P 2021 Wilton ripples in weakly nonlinear models of water waves: existence and computation *Water Waves* **3** 491–511
- [7] Akers B and Nicholls D P 2021 Wilton ripples in weakly nonlinear dispersive models of water waves: existence and analyticity of solution branches *Water Waves* **3** 25–47
- [8] Schwartz L W and Vanden-Broeck J-M 1979 Numerical solution of the exact equations for capillary-gravity waves *J. Fluid Mech.* **95** 119–39
- [9] Ellen Haupt S and Boyd J P 1988 Modeling nonlinear resonance: a modification to the Stokes' perturbation expansion *Wave Motion* **10** 83–98
- [10] Reeder J and Shinbrot M 1981 On Wilton ripples, I: formal derivation of the phenomenon *Wave Motion* **3** 115–35
- [11] Reeder J and Shinbrot M 1981 On Wilton ripples, II: rigorous results *Arch. Ration. Mech. Anal.* **77** 321–47
- [12] Langer R, Trichtchenko O and Akers B 2024 Wilton ripples with high-order resonances in weakly nonlinear models *Water Waves* **6** 1–30
- [13] Creedon R 2024 Existence of all Wilton ripples of the Kawahara equation (arXiv:2411.13508 [math.AP])
- [14] Henderson D M and Hammack J L 1987 Experiments on ripple instabilities. Part 1. Resonant triads *J. Fluid Mech.* **184** 15–41
- [15] Perlin M, Henderson D and Hammack J 1990 Experiments on ripple instabilities. Part 2 selective amplification of resonant triads *J. Fluid Mech.* **219** 51–80
- [16] McGoldrick L F 1970 An experiment on second-order capillary gravity resonant wave interactions *J. Fluid Mech.* **40** 251–71
- [17] Trichtchenko O, Deconinck B and Wilkening J 2016 The instability of Wilton ripples *Wave Motion* **66** 147–55
- [18] Akers B and Nicholls D P 2013 Spectral stability of deep two-dimensional gravity-capillary water waves *Stud. Appl. Math.* **130** 81–107
- [19] Akers B F 2015 Modulational instabilities of periodic traveling waves in deep water *Physica D* **300** 26–33
- [20] Creedon R, Deconinck B and Trichtchenko O 2021 High-frequency instabilities of the Kawahara equation: a perturbative approach *SIAM J. Appl. Dyn. Syst.* **20** 1571–95
- [21] Creedon R P, Deconinck B and Trichtchenko O 2022 High-frequency instabilities of Stokes waves *J. Fluid Mech.* **937** A24
- [22] Martin C I and Matioc B-V 2013 Existence of Wilton ripples for water waves with constant vorticity and capillary effects *SIAM J. Appl. Math.* **73** 1582–95

- [23] Ehrnström M, Escher J and Wahlén E 2011 Steady water waves with multiple critical layers *SIAM J. Math. Anal.* **43** 1436–56
- [24] Ehrnström M, Johnson M A, Maehlen O I H and Remonato F 2019 On the bifurcation diagram of the capillary-gravity Whitham equation *Water Waves* **1** 275–313
- [25] Akers B F and Ambrose D M 2025 Internal capillary-gravity wilton ripples *Water Waves* (<https://doi.org/10.1007/s42286-025-00112-x>)
- [26] Akers B F, Ambrose D M and Sulon D W 2019 Periodic travelling interfacial hydroelastic waves with or without mass II: multiple bifurcations and ripples *Eur. J. Appl. Math.* **30** 756–90
- [27] Baldi P and Toland J F 2010 Bifurcation and secondary bifurcation of heavy periodic hydroelastic travelling waves *Interfaces Free Bound.* **12** 1–22
- [28] Berger K M and Milewski P A 2000 The generation and evolution of lump solitary waves in surface-tension-dominated flows *SIAM J. Appl. Math.* **61** 731–50
- [29] Trichtchenko O, Deconinck B and Kollár R 2018 Stability of periodic traveling wave solutions to the Kawahara equation *SIAM J. Appl. Dyn. Syst.* **17** 2761–83
- [30] Boyd J P 1991 Weakly non-local solitons for capillary-gravity waves: fifth-degree Korteweg-de Vries equation *Physica D* **48** 129–46
- [31] Akers B and Milewski P A 2009 A model equation for wavepacket solitary waves arising from capillary-gravity flows *Stud. Appl. Math.* **122** 249–74
- [32] Diorio J D, Cho Y, Duncan J H and Akylas T R 2011 Resonantly forced gravity–capillary lumps on deep water. Part 1. Experiments *J. Fluid Mech.* **672** 268–87
- [33] Moldabayev D, Kalisch H and Dutykh D 2015 The Whitham equation as a model for surface water waves *Physica D* **309** 99–107
- [34] Mikyoung Hur V and Johnson M A 2015 Modulational instability in the Whitham equation with surface tension and vorticity *Nonlinear Anal.: Theory Methods Appl.* **129** 104–18
- [35] McGoldrick L F 1970 On Wilton’s ripples: a special case of resonant interactions *J. Fluid Mech.* **42** 193–200
- [36] Phillips O M 1981 Wave interactions—the evolution of an idea *J. Fluid Mech.* **106** 215–27
- [37] Hammack J L and Henderson D M 1993 Resonant interactions among surface water waves *Annu. Rev. Fluid Mech.* **25** 55–97
- [38] Craik A D D 1988 *Wave Interactions and Fluid Flows* (Cambridge University Press)
- [39] Chow C C, Henderson D and Segur H 1996 A generalized stability criterion for resonant triad interactions *J. Fluid Mech.* **319** 67–76
- [40] Bretherton F P 1964 Resonant interactions between waves. The case of discrete oscillations *J. Fluid Mech.* **20** 457–79
- [41] Claassen K M and Johnson M A 2018 Numerical bifurcation and spectral stability of wavetrains in bidirectional Whitham models *Stud. Appl. Math.* **141** 205–46